Journal of Applied Physics

Humidity-induced significant microstructural reordering in partially reduced graphene oxide: Insights on water permeation mechanism

Cite as: J. Appl. Phys. **125**, 024303 (2019); https://doi.org/10.1063/1.5078665
Submitted: 27 October 2018 . Accepted: 06 December 2018 . Published Online: 09 January 2019

T. M. Pranav, Tushar Sakorikar, Pramitha Vayalamkuzhi, and Manu Jaiswal

Journal of Applied Physics ARTICLE scitation.org/journal/jap

Humidity-induced significant microstructural reordering in partially reduced graphene oxide: Insights on water permeation mechanism

Cite as: J. Appl. Phys. **125**, 024303 (2019); doi: 10.1063/1.5078665
Submitted: 27 October 2018 · Accepted: 6 December 2018 ·
Published Online: 9 January 2019

T. M. Pranav,[1,a)] Tushar Sakorikar,[1,2,a)] Pramitha Vayalamkuzhi,[2,a)] and Manu Jaiswal[1,a),b)]

AFFILIATIONS

[1]Department of Physics, Indian Institute of Technology, Madras, Chennai, India
[2]Department of Electrical Engineering, Indian Institute of Technology, Madras, Chennai, India

[a)]The manuscript was written through contributions of all authors. All authors have given approval to the final version of the manuscript. T. M. Pranav and T. Sakorikar contributed equally to this work.
[b)]**E-mail:** manu.jaiswal@iitm.ac.in

ABSTRACT

Interaction of water and water-based solvents with graphene oxide (GO) has attracted much attention, due to the ability of GO to serve as a highly effective water filtration membrane. In this work, we study the evolution of the structure of GO in a partially reduced form, before and after being hydrated in high humidity conditions. X-ray diffraction (XRD) studies reveal that progressive thermal reduction leads to the increase in the microstructural disorder in the stacking of GO flakes. However, upon hydration of partially reduced GO, microstructural ordering is revealed. This ordered state is characterized by two XRD peaks with substantially smaller full-width-at-half-maximum (FWHM), when compared to the pre-hydration state. The peak corresponding to the sp^3 regions has larger d-spacing of ~9.7 Å and an FWHM ~6 times smaller compared to pre-hydration state, while the other peak corresponds to the ordered sp^2 regions with a d-spacing of ~3.3 Å, observed at the characteristic graphitic peak position. Gravimetry studies on suspended films reveal both accelerated and diminished water permeation rates upon annealing when compared to unreduced GO films, which can be attributed to void-assisted permeation in the microstructurally disordered films. The hydrated films in a similar way show a permeation behavior that involves either the increase or decrease in water permeation rates in comparison with pre-hydrated samples. We reconcile to the gravimetry outcomes by suggesting the possibilities of both super-permeating channels and void assisted permeation, and the contribution of each of the mechanisms to the permeation flux.

I. INTRODUCTION

Graphene oxide (GO) has shown its potential to act as a superior water purification membrane[1,2] or selective ion rejection membrane.[3–5] This ability is further aided by the fact that GO membranes require facile preparation route,[6] and they can easily be scaled up, being solution processable.[7] Its application as a purification or filtration membrane has been possible due to its unique interaction with water. The laminates of GO contain trapped water, hydrogen bonded to the functional groups, and mobile water, with the latter being present in the interspersed sp^2-rich network of GO nano-capillaries.[8,9] Water transport through GO is a very interesting phenomenon due to the preference of graphene oxide (GO) for transporting water over other lighter nuclei like helium, as reported by Nair *et al.*[1] In the same study, it was proposed that water super-permeates through GO membranes, caused by the frictionless flow of water between the GO laminates. These GO laminates swell upon being exposed to humid environment, leading to variation in the d-spacing as reported in both experimental and simulation-based studies.[10–12] Such a variation was also found

for GO films immersed in solvents, and further it had a dependence on temperature and polarity of the solvent.[13,14] This variation in the interlayer spacing was used to develop membranes that can selectively reject ions in an aqueous solution.[3]

Though GO has been shown to be a promising material for water filtration and ion sieving applications, the mechanism of permeation of water through GO membranes is still unclear and the research community lacks agreement on a single theory. In the same concern, there are three theories or models that present a conflicting picture of water permeation in GO. It is believed that the discrepancies have to do with variations in the functional groups[15] and the microstructural arrangements of GO.[16] One of the first models suggested frictionless flow of water through the circuitous pathways in GO laminates results in super-permeation. According to this model, the hydrophilic regions in GO nano-capillaries act as spacers that maintain the interlayer spacing (≥5 Å) required to accommodate a monolayer of water, while the hydrophobic regions within these hydrophilic areas are responsible for the observed fast water transport.[1] Another report hypothesized the presence of microstructural defects or voids within GO laminates, which were held to be responsible for water permeation, rather than the super-permeation process through nano-capillaries.[17] The study indicated that GO membranes are prone to have a dynamic microstructure which can significantly alter the water flux through the film. A severe reduction in the water permeation has been reported due to the compaction of the loose microstructure. It has also been conferred that cavities and other defects dominate the permeation flux over hydrophobic graphitic regions in the GO lamina. Further, it has also been demonstrated that a favorable permeation flux can be obtained by the slow deposition of the film which leads to the self-assembly of GO flakes.[2] In a recent report by Saraswat *et al.*,[18] the permeation of water through GO laminates was ascribed to defects or pin-holes on the GO flakes and/or the microstructural arrangement of the GO flakes in the membrane. Had water super-permeation through nanocapillary networks been the primary process, they argued, then a significant dependence on the flake size of GO may be expected. However, such dependence was not observed.[18] The latter reports converge to the fact that the water permeation flux has a strong dependence on the inherent microstructure of GO. Thus, the explanation of water permeation rates through GO is not well settled. Prolonged exposure of unreduced GO to different relative humidities has been used to tune the *d*-spacing in a continuous manner,[3] and further it has also led to reversible changes in the GO microstructure.[17] However, in both these reports, the X-ray diffraction (XRD) data do not reveal any significant change in the full-width-at-half-maximum (FWHM) or peak intensity upon humidity exposure. Both these parameters are direct manifestations of any significant changes in GO microstructure. In the work of Chong *et al.*,[17] the reversible nature of the microstructural transition upon a cycle of hydration precludes the possibility of recording this through X-ray studies, unless probed *in situ*. Thus, only a gradual time-dependent decrease in XRD peak intensity is observed for films stored in ambient conditions. We therefore considered looking for alternate oxidation states of GO or for other processing conditions, where distinct microstructural changes are revealed upon hydration. In this work, we show substantial ordering in the microstructure of partially reduced GO, as measured using X-ray diffraction studies, after a cycle of hydration. The GO samples were annealed at T = 150 °C. The annealed samples were then subjected to prolonged humidification, which upon hydration showed strong ordering in all the samples as revealed in both substantial reduction of FWHM corresponding to the sp^3 regions, increase of peak intensity and its shift to higher *d*-spacing, as well as emergence of a clear graphitic peak. Water permeation is discussed in light of significant changes in the GO microstructure and *d*-spacing, both due to thermal reduction of GO and due to hydration of partially reduced GO.

II. METHODS

A. Sample preparation

A GO dispersion in water (4 mg/ml) purchased from University Wafer, which had an elemental composition of carbon ~49%-56% and oxygen ~41%-50%, was used in this study. The aqueous dispersion of GO was then diluted to 2 mg/ml by adding equal amount (vol/vol%) of ethanol to the parent solution. The solution was then spin-coated on quartz substrates to obtain uniform films of identical thickness. Before spin coating, the substrates were treated with oxygen plasma to make the surface hydrophilic. For reduction of GO films, thermal annealing in an argon atmosphere was performed at different temperatures. The average thickness of the films as measured by Bruker Contour GT 3D optical profilometer was found to be 500 ± 50 nm. These films were then characterized with X-ray diffraction (XRD), X-Ray Photoelectron Spectroscopy (XPS), and Fourier-Transform Infrared (FTIR) spectroscopic studies. GO, GO-150, and GO-150-H denote as-prepared, 150 °C annealed, and 150 °C annealed and hydrated films, respectively.

B. Gravimetric studies

Free-standing GO membranes were prepared to perform gravimetry experiments. GO dispersion in ethanol-water was spin coated onto a copper foil (GoodFellow, thickness: 25 μm) after the foil was treated with oxygen plasma. An opening of 16 mm^2 was created in the copper foil by selectively etching it from the center using ammonium peroxodisulfate to obtain free-standing GO membrane. The as-prepared membranes on copper foil are then placed and sealed on a copper container using a gasket maker, a high temperature RTV (Room Temperature Vulcanising) silicone ensuring that the permeation occurs only through the suspended GO, GO-150, and GO-150-H film. Before sealing, water was filled inside the copper cup, which was then heated to ~60 °C and the weight loss was monitored at regular time intervals.

III. RESULTS AND DISCUSSION

Figure 1(a) shows the SEM image of GO flakes spin coated over a Si/SiO_2 substrate cast from an extremely dilute dispersion of GO to evaluate the flake size distribution. The GO flake size is found to be $3 \pm 1\,\mu$m (as calculated using ImageJ software). Much thicker and continuous films using a higher concentration of GO dispersion spin-coated at much lower spin speed were obtained for other experiments performed in this work. Figure 1(b) shows the Raman spectra of GO film, showing characteristic "G" peak at 1598 cm^{-1} and "D" or defect peak at 1337 cm^{-1}. The defect peak arises due to presence of oxygen functionalities in the GO. Thermal reduction is one of the methods to remove these defects from GO. However, reducing GO thermally also leads to structural changes. To evaluate these structural changes, GO was annealed at different temperatures and X-ray diffraction (XRD) was performed subsequently. The variation in the XRD peaks as a function of the annealing temperature can be seen in Fig. 2(a). A moving average filter was used to smoothen out the baseline corrected plot for clarity of presentation. The c-axis separation decreased upon annealing which can be inferred from the increase in the 2θ value from 10.61° to 18.62°. This is consistent with the XRD studies of GO found in various other papers.[8,19] The FWHM of the peaks is of considerable interest as it sheds more light about the inherent order in the microstructure of GO. It is observed that for annealing temperatures from 120 °C to 140 °C, the FWHM broadened dramatically (see Table I). Since the observed broadening is significant, it is indicative of the fact that GO microstructure becomes increasingly disordered upon thermal annealing at these temperatures.

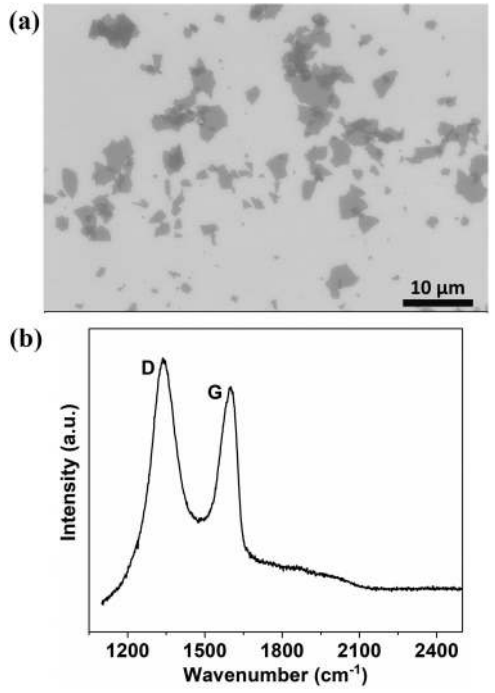

FIG. 1. (a) SEM micrograph of GO flakes. (b) Raman spectra of GO with characteristic "G" peak and "D" peak.

The Scherrer equation gives an estimate of the average crystallite size (τ) of the system in terms of the Bragg angle (θ) and FWHM (β), $\tau = K\lambda/\beta\cos\theta$, where $K \sim 0.9$ and λ is the X-ray wavelength. Assuming this equation to be valid, the average number of GO flakes stacked in one vertical crystallite is found to be 15 for as-prepared GO. The mean crystallite size decreases to a value close to 9 for GO annealed at 150 °C, with the change happening entirely between the temperature interval of 120 °C and 140 °C. Thus, there is a clear reduction in the mean crystallite size by a factor of more than 1.5. We also note that the reduction of the intensity by a factor of 20 is not compensated by the larger spread indicating that there is a reduction in the mean crystallite size upon annealing. Thus, we can ascertain the possibility of a more loosely and randomly arranged microstructure as the temperature increases. Interestingly, this change can predominantly be attributed to the expulsion of water which is consistent with the previous literature where Fourier Transform Infra-Red (FTIR) spectroscopy studies and ellipsometry studies have been conducted on these annealed samples that verify the same observation.[8,20] These observations thus strongly suggest that water plays an important role in determining the microstructure of GO.

To further build on this hypothesis, water was reintroduced into the system while ensuring minimum elimination of the functional groups. Samples annealed at 150 °C were chosen as these are partially reduced samples which still retain the functional groups present in GO to a large extent.[8,21,22] To that effect, these samples were exposed to high humidity (RH > 95%) for prolonged period (24 h). Under this highly humid condition, the XRD peak present at ~15° was shifted back to a 2θ value of 9.1° corresponding to a d-spacing of ~9.7 Å. Furthermore, an additional peak at ~27° was observed corresponding to a graphitic d- spacing of 3.3 Å, as can be seen in Fig. 2(b). The FWHM of the 9.1° peak was ~0.246 which is 2.5 times lesser than that of the original GO peak at room temperature as well as it is ~6 times lesser than the pre-hydration state. Both these comparisons indicate a strong ordering of the GO flakes under highly humid conditions. The average number of GO flakes per crystallite was found to increase by 4-fold to 37 upon hydration of GO-150 samples. Alternate data sets for 2 more samples are available in S1 in the supplementary material. As can be seen in Fig. 2(b), the presence of a new peak at ~27° derives considerable interest. This peak, which translates to the pure graphitic peak, shows that there has been an ordering of the pure sp^2 regions which were present randomly in the initial GO system along with the new regions produced due to annealing. This leads to the conclusion that interaction with water can play an important role in restoring structural order between the GO flakes.

To provide a better understanding of the aforementioned observations, a toy model has been simulated (using MatlabR2018a software) to quantify the order between the

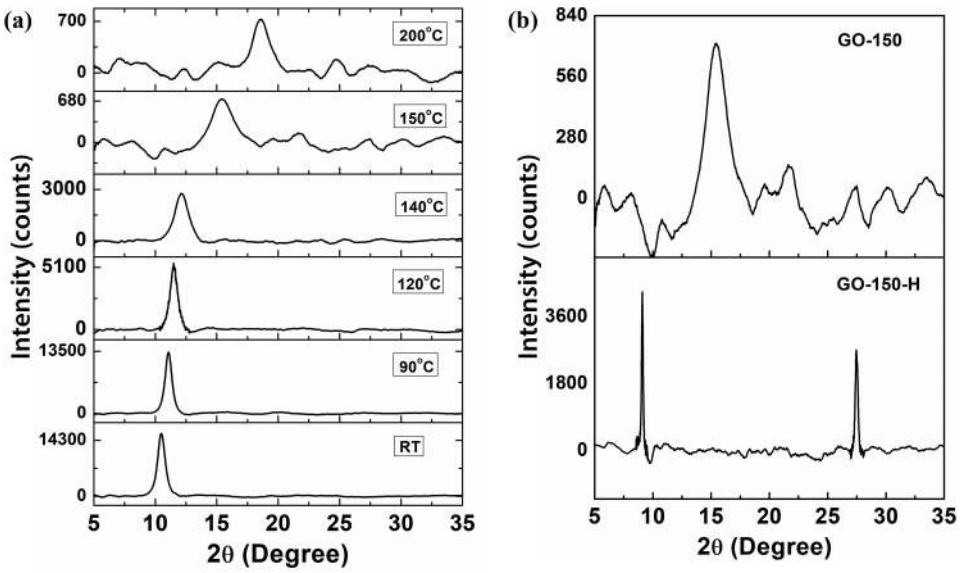

FIG. 2. (a) Comparison of X-ray diffraction (XRD) spectra of GO at room temperature and annealed up to 200 °C. (b) Comparison of XRD spectra of GO annealed at 150 °C before and after hydration.

GO flakes. In the case of crystalline samples, the average number of flakes that form a crystallite (N) was determined using the "Scherrer equation," which is an approximation of the structure factor. The mean crystallite size thus obtained has been discussed in the previous paragraph. The Scherrer equation, however, assumes a single-value defining the crystallite size, rather than a distribution of crystallite size. Moreover, even for the single crystallite size, the formula may not be completely valid for very small crystallite sizes, which is the case here. Since both the number of flakes contributing to a crystallite and the distribution of the crystallites in the entire GO film itself is unknown, we look for a more refined approach that can also reveal the distribution of these in GO. A detailed discussion of this approach is presented in S2 in the supplementary material.

In this regard, we assume a distribution of ordered vertical stacks of GO flakes whose internal *d*-spacing corresponds to the mean *c* axis separation obtained from the XRD peak positions. Each stack consists of GO flakes that are arranged in such a way that the spacing between them is uniform and several such stacks together make up the GO film assuming that the spacing between two stacks is random. We denote a vertical stack of GO flakes by the number of ordered GO flake layers present within a stack which is represented by "N." The microstructural disorder in the system is captured in the fact that the separation between two ordered stacks is random and thus would contribute incoherently to the XRD peak.

TABLE I. XRD characteristics of GO annealed at different temperatures.

Temperature (°C)	Peak (2θ)	Intensity (counts)	FWHM (2θ)	d-spacing (Å)
30[a]	10.61	12 720	0.615	8.33
90	10.86	9657	0.617	8.14
120	11.69	3712	0.604	7.56
140	14.3	867.4	1.67	6.18
150	15.47	1197.3	1.52	5.72
200	18.62	826.4	1.47	4.76

[a]Room temperature (RT).

When the lattice contribution to X-ray intensity or the structure factor is computed for very thin crystallites, then the fundamental relation[23]

$$|S_N|^2 \propto \left(\frac{\sin\left(\frac{N\theta}{2}\right)}{\sin\left(\frac{\theta}{2}\right)}\right)^2 \quad (1)$$

is more useful. Here, S_N is the structure factor from "N" flakes of GO contributing to one vertical stack forming the crystallite. The total intensity arises from the contributions from many crystallites of varying sizes given by

$$I \propto |F(Q)|^2 \left(\sum_j |S_{N_j}|^2 + \sum_{\substack{j,k \\ j \neq k}} S_{N_j}.S^*_{N_k}\right), \quad (2)$$

where $F(Q)$ is the unit cell contribution, S_{N_j} is the structure factor of *j*th stack, and $(S_{N_j}.S^*_{N_k})$ are the product terms of the structure factor due to *j*th stack and *k*th stack, respectively. The second term in the parenthesis on the right-hand side of Eq. (2) averages to zero, as interference term from different

crystallites is incoherent [see S2 (c) in the supplementary material for more details]. The model involves varying "N" to get a "single" integer value, N_{med}, for flake number per crystallite that best reproduces the experimental FWHM. Having obtained N_{med}, a distribution of flake size about N_{med} is simulated that further lowers the deviation of FWHM from experimental values [see S2 (d) in the supplementary material for an elaborate description]. We assign $\sum_j N_j d = t$, where "N_j" is the number of ordered GO flakes in the jth vertical stack, "d" is the vertical flake separation for the given oxidation state, and "t" is the total film thickness. A distribution of the various crystallite sizes such that the total produces the experimentally observed FWHM for the given d-spacing is simulated. Figures 3(a)–3(c) show the comparison of the distribution of crystallites in GO, GO-150, and GO-150-H, respectively. Count indicates the number of times a crystallite size is present in the GO system. To get a better statistic, the process was iterated 100 times and the total count for each crystallite size is reported in the above simulated graphs.

To present an overview, the distribution plotted over the bar graphs indicates the likelihood of a particular crystallite size to appear in the GO system. It is clear from the simulations that the number of GO flakes in an ordered stack present in the GO system [Fig. 3(a)] reduces upon thermal annealing at 150 °C due to distortion of inter-flake arrangement [Fig. 3(b)]. This is also reflected in the FWHM of the XRD peaks. However, upon hydration the number of ordered flakes or crystallites stacked up, increase by six to seven times on an average [Fig. 3(c)]. Identical conclusion can also be drawn by direct use of Scherrer equation; its limitation notwithstanding. The average crystallite size obtained from Scherrer equation is indicated with a red arrow and is close to the peaks of the distribution obtained from the toy model [see Figs. 3(a)–3(c)]. These differences in the microstructure of GO, GO-150, and GO-150-H are schematically represented in Fig. 3(d). In the case of GO, there exists an ordered stacking of sp^3 domains, which gets disrupted upon thermal annealing. Due to thermal annealing, the mean crystallite size is reduced, indicating disorder in the microstructure. Upon hydration, the XRD reveals that the order is restored for both sp^3- and sp^2-rich regions. This aspect is quantitatively captured in the toy model, which reveals a higher number of flakes in the ordered stacks present in GO-150-H followed by GO and GO-150.

Since the XRD analysis reveals strong ordering of the microstructure upon hydration of 150 °C annealed sample, it is instructive to evaluate if any accompanying changes in the chemical structure or chemical environment are involved. Toward this, X-ray Photoelectron Spectroscopy (XPS) was performed on the annealed (GO-150) and subsequently hydrated samples (GO-150-H). The XPS peaks were deconvolved using the software XPSPEAK 4.1 software, and the individual peaks were fitted with a mixture of Lorentzian and Gaussian. Figure 4(a) shows the carbon peak of GO-150 that has binding energy values of 284.5, 286.5, and 289.07 eV corresponding to (C—C, C—H), (C—OH, C—O—C), and (O—C=O),

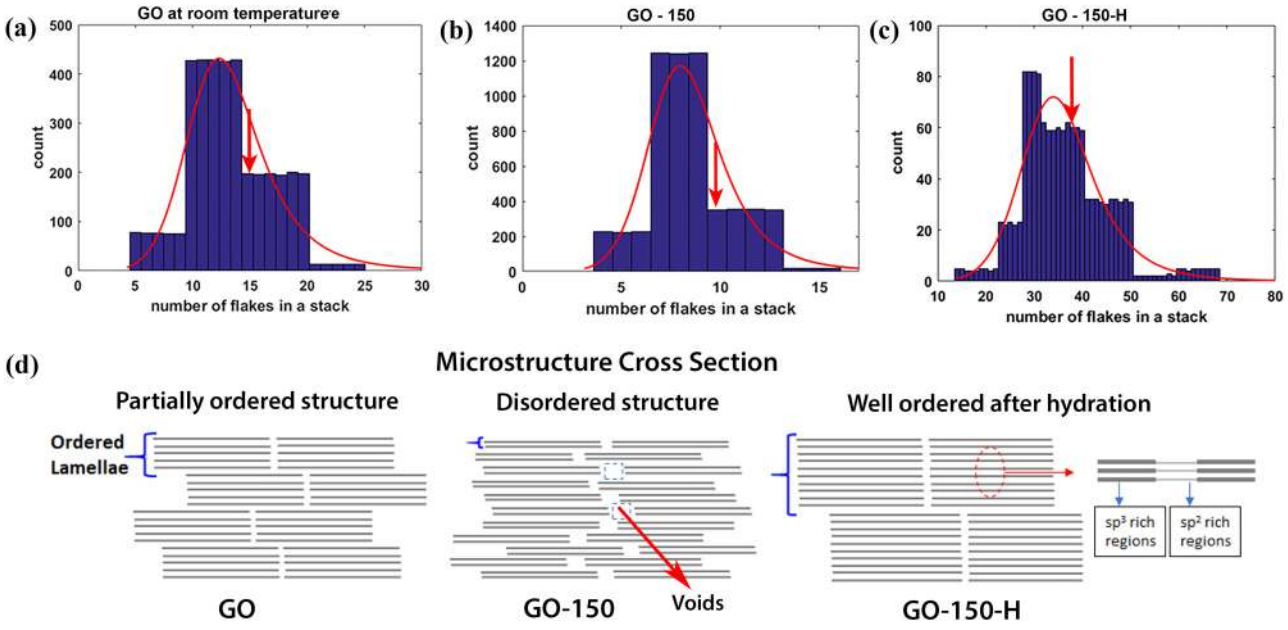

FIG. 3. Comparison of the estimated number of flakes in an ordered form for (a) GO, (b) GO-150, and (c) GO-150-H [the red arrows in (a)–(c) indicate the values of average number of flakes (crystallites) in a stack obtained from Scherrer equation]. (d) Schematic representation of proposed variation in microstructure of GO, GO-150, and GO-150-H.

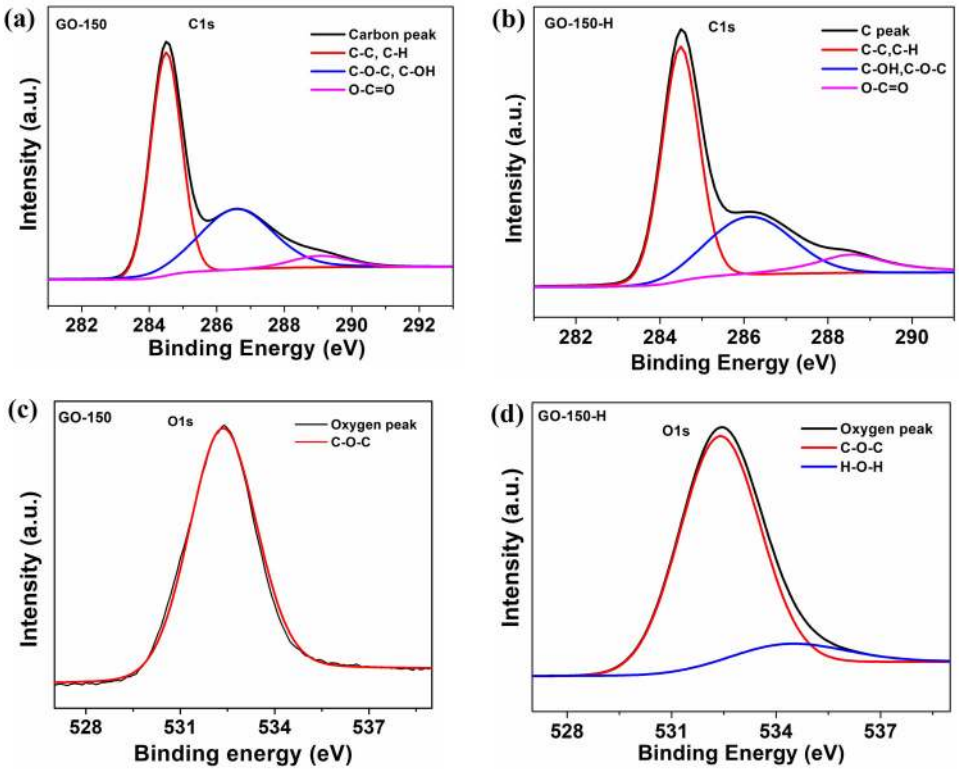

FIG. 4. High resolution C1s core-level spectra of (a) GO-150 and (b) GO-150-H. High resolution O1s core-level spectra of (c) GO-150 and (d) GO-150-H.

respectively.[24] The carbon peak of GO-150-H had a similar deconvolution with binding energies of 284.5, 286.3, and 288.5 eV, respectively, for the aforementioned functional groups [see Fig. 4(b)]. Notable variations in the oxygen peak characteristics are seen for the GO-150 and the GO-150-H samples. While the oxygen peak of GO-150 had a single peak at 532.4 eV corresponding to (C—O—C, C—OH) groups, the GO-150-H had an additional peak at 534.4 eV corresponding to (H—O—H)[24,25] along with the standard (C—O—C, C—OH) peak at 532.2 eV, as evident from Figs. 4(c) and 4(d). Thus, from the XPS spectra, it is clear that the GO-150-H sample contains water. It is striking that even though XPS is performed in ultra- high vacuum, the presence of the water peak albeit at lower intensity implies that some water which is intercalated between graphene oxide sheets is still present. The abnormally large FWHM is also associated with water intercalated GO sheets, wherein the photoelectrons coming out of oxygen are in an environment facing a large local potential of highly polar water molecule.[26,27] Therefore, the large spread in FWHM posited due to increased variations in the kinetic energy of the electron caused largely by the huge variation in the potentials is justified. XPS studies thus indicate the modified chemical environment of GO-150 upon hydration as revealed by the presence of the intercalated water subsequent to the water vapor exposure.

An additional probe on the chemical structure is FTIR. Figure 5(a) compares the FTIR spectra of GO-150 and GO-150-H. A major difference in the spectra before and after hydration is the presence of a prominent peak at 1635 cm^{-1} in GO-150-H, corresponding to the —OH bending modes of water.[28] This confirms the presence of intercalated water in GO-150-H, consistent with the observations made from XPS spectra.

The spectra also reveal that the process of hydration did not induce any other compositional changes as evident by the absence of any new peak in spectrum of GO-150-H, when compared to that of GO-150. The ability of intercalated water to transform the microstructure of the GO is particularly intriguing in the context of the ability of GO membranes to transport water. It was initially reported that GO membranes have the ability to rapidly transport water through sp^2 rich network of nanocapillaries, with diffusion constant being 10^4 times that of bulk water.[1] However, recent works have contested that the permeability of water through GO depends on these hydrophobic channels and instead argue that the flow is governed largely by the presence of voids.[17,18] The partially reduced GO with its complete transformation of microstructure, obtained in our studies, is therefore an ideal test-system to address this question. We thus decided to record the

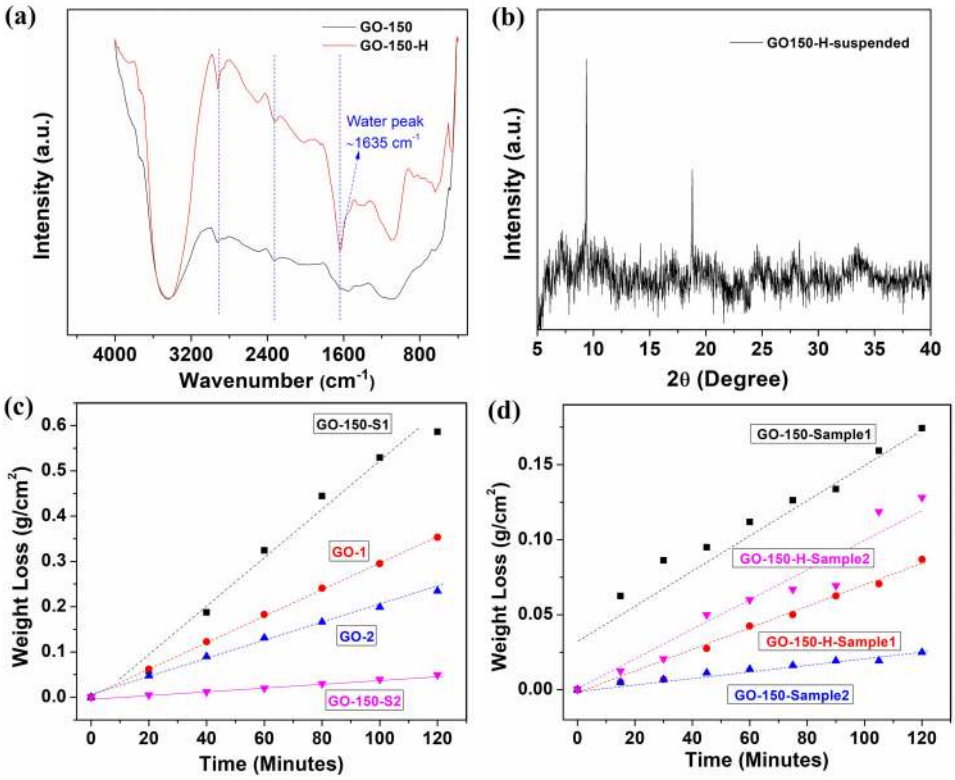

FIG. 5. (a) XRD spectra of GO-150-H post hydration and gravimetry experiment. (b) Comparison of FTIR spectra of GO-150 and GO-150-H. (c) Comparison of normalized weight loss with time between different samples of GO and GO-150. (d) Weight loss results comparing GO-150 and GO-150-H for two sets of samples.

permeation flux of water through suspended membranes of disordered (GO-150) and water induced structurally ordered samples of GO (GO-150-H). So far, the microstructural ordering has been discussed in the context of partially reduced GO on substrates. In context of the gravimetry experiments, we also studied the microstructural changes in the suspended GO-150 membranes upon hydration. To understand these microstructural changes on suspended GO-150 films, XRD studies were performed on GO-150-H membranes post gravimetry experiments. Figure 5(b) shows the XRD spectra of GO-150 post 24 h hydration and 2 h gravimetry. Two sharp peaks at 9.36° and 18.78° are observed corresponding to d-spacings of 9.43 Å and 4.72 Å, respectively. This observation was consistent across different samples (see S3 in the supplementary material for alternate data set). The results from XRD on hydrated suspended samples again confirm the reordering of the microstructure that was discussed above for supported GO-150 upon hydration [see Fig. 2(b)].

We now discuss the observations from the gravimetry experiments. We first compare the water permeation rates for GO and GO-150 samples. Figure 5(c) shows the weight loss as a function of time for two representative sets of GO and GO-150 samples, namely GO-1, GO-2, and GO-150-S1, GO-150-S2, respectively. GO-150-S1 has an average permeation rate of 4.60×10^{-3} g min^{-1} cm^{-2}, followed by that of GO-1, GO-2, and GO-150-S2, which is 2.95×10^{-3} g min^{-1} cm^{-2}, 1.98×10^{-3} g min^{-1} cm^{-2}, and 4.06×10^{-4} g min^{-1} cm^{-2}, respectively. We thus observe that water permeation rates across GO-150 and GO samples showed a mixed behavior, rather than a defining trend. To evaluate the effect of hydration of GO-150 sample on its water permeation behavior, we now compare the results from gravimetry experiments performed on suspended GO-150 and GO-150-H films. Figure 5(d) shows the comparison of weight loss through two representative sets of GO-150 and GO-150-H samples. Permeation rates observed are 1.45×10^{-3} g min^{-1} cm^{-2} and 7.24×10^{-4} g min^{-1} cm^{-2} for GO-150-Sample1 and GO-150-H-Sample1, respectively, indicating higher permeation in GO-150 when compared to GO-150-H, while for another set the observed permeation rates are 2.15×10^{-4} g min^{-1} cm^{-2} and 1.07×10^{-3} g min^{-1} cm^{-2} for GO-150-Sample2 and GO-150-H-Sample2, respectively, showing the reverse trend when compared to that observed in other set of samples. To summarize the observations: gradual microstructural disordering happens in GO upon reduction and a dramatic microstructural ordering upon subsequent hydration. However, the

water permeation rates through suspended GO membranes do not show clear trend both before and after partial reduction and also upon hydration of partially reduced GO.

We now discuss the results from gravimetry experiments performed on GO, GO-150, and GO-150-H in light of the differences in their microstructure as understood from the XRD spectra. From the gravimetry data for GO and GO-150, we infer that GO-150 sample, despite having smaller d-spacing (see Table I) compared to that observed for GO, shows permeation rates which are both lower and higher than the latter across different samples. Also, it should be noted that partial reduction of GO at 150 °C leads to the substantial loss of intercalated water present in between GO flakes, as discussed in previous studies.[8,21] These observations gain importance considering the early work on water permeation by Nair *et al.*,[1] which suggested that both higher d-spacing and the intercalated water contribute to the super permeation of water as observed for GO, whereas in our case even for partially reduced GO (GO-150), similar or higher water permeation rates are observed compared to that for GO. This indicates that there is a factor different from the aforementioned ones that affects the water transport through the GO-150 sample. With reference to the XRD data obtained for GO-150 sample that suggests disorder in the microstructure, we ascribe this mixed behavior of water permeation to the presence of voids within the GO-150 microstructure. The presence of voids has been recently proposed elsewhere in the literature for the cases of as prepared GO.[17,18] The difference between the microstructure of GO and GO-150 is further elaborated in the schematic shown in Fig. 3(d). We suggest that the mixed water permeation behavior observed between GO and GO-150 can be attributed to two competing mechanisms: (i) resistance offered by the smaller d-spacing and loss of intercalated water which results in lowering the permeation rate; (ii) the presence of voids in the microstructure of GO-150 that promotes the water transport.

Similarly, we can also reconcile to the water permeation behavior as observed for GO-150 and GO-150-H samples from gravimetry. The XRD data clearly reveal the presence of more order in GO-150-H samples, confirming the fact that hydration clearly brings structural order to partially reduced GO. The fact that water likes to sandwich in between two sp^3 rich regions is confirmed by the free energy studies as discussed in a report by Maiti *et al.*[29] As GO-150-H assumes a far more ordered phase, we suggest that the presence of voids has decreased, and thus if we assume a void assisted water permeation mechanism, we can expect the permeation to have a lower rate when compared to the pre-hydrated state. But it is worth noting that a strong ordering also provides provision for a greater number of uninterrupted channels (ordered sp^3 rich regions) that can promote water permeation through the channels. The fact that we are able to obtain both higher and lower permeation fluxes for GO-150-H, when compared to GO-150 sample, convinces the need to evaluate respective dominance of the two competing factors on a sample-by-sample basis. Now considering the hydrated sample, it is important to note from comparison of FTIR spectra of GO-150 and GO-150-H [Fig. 5(a)] that there is a negligible change in the functional groups after hydration, except for the prominent water peak observed for GO-150-H. This provides further evidence that partially reduced GO can still intercalate water upon hydration. The process of hydration also leads to an ordered stacking in the sample along with a larger d-spacing in ambient (50% RH) conditions (9.62 Å for GO-150-H) compared to not only the pre-hydrated sample but also pristine GO (d-spacing—8.33 Å), providing spacers for a larger water flux. This is an important observation to note that despite of reproducing the required nano-channels of widths similar to GO (due to increased d-spacing), the permeation flux in GO-150-H water conduction did not increase beyond the values observed for GO. This observation suggests that water permeation cannot be solely attributed to the super-permeating channels. We, nonetheless, also cannot argue that it is only the presence of voids that altogether dominates the permeation rates, since we observe a distinct increase in the permeation rates of some of the samples of GO-150-H over GO-150, which should not have been the case if it were governed only by voids. We, therefore, hypothesize that it is an optimized number of voids and super-permeating channels that assist water permeation through GO and partially reduced GO.

IV. CONCLUSION

Graphene oxide is characterized by dynamic microstructure. The structure of GO gets modified and becomes disordered microscopically upon thermal reduction, as the functional groups are removed gradually, leading to the creation of defects. In this work, we show that a significant ordering can be induced in the disordered structure of partially reduced GO upon prolonged exposure to high humidity conditions. Further, we also observe that reordering happens both for suspended and supported samples.

It is a well-studied phenomenon that microstructure of GO governs its ability to intercalate water as well as water transport through it. Our study reveals that both GO microstructure and water intercalation are mutually dependent. Our study thus helps address the recently contested arguments on the dominant water transporting mechanism through GO. We show that both water transport through GO nanocapillaries and that through voids play an important role in governing the water flow rate through GO and partially reduced GO membranes.

SUPPLEMENTARY MATERIAL

Supplementary material contains additional XRD data for both supported and suspended GO-150 samples before and after hydration. Further, a detailed mathematical description on the X-ray diffraction toy model is presented.

ACKNOWLEDGMENTS

We would like to acknowledge CeNSE, IISc for XPS measurements and SAIF, IIT Madras, for FTIR studies. We also acknowledge CNNP, IIT Madras (an initiative by DeitY, Government of India), for surface profilometry measurements.

REFERENCES

[1]R. R. Nair, H. A. Wu, P. N. Jayaram, I. V. Grigorieva, and A. K. Geim, Science **335**(6067), 442 (2012).
[2]W. L. Xu, C. Fang, F. Zhou, Z. Song, Q. Liu, R. Qiao, and M. Yu, Nano Lett. **17**(5), 2928–2933 (2017).
[3]J. Abraham, K. S. Vasu, C. D. Williams, K. Gopinadhan, Y. Su, C. T. Cherian, J. Dix, E. Prestat, S. J. Haigh, I. V. Grigorieva, P. Carbone, A. K. Geim, and R. R. Nair, Nat. Nanotechnol. **12**, 546 (2017).
[4]R. K. Joshi, P. Carbone, F. C. Wang, V. G. Kravets, Y. Su, I. V. Grigorieva, H. A. Wu, A. K. Geim, and R. R. Nair, Science **343**(6172), 752–754 (2014).
[5]L. Chen, G. Shi, J. Shen, B. Peng, B. Zhang, Y. Wang, F. Bian, J. Wang, D. Li, Z. Qian, G. Xu, G. Liu, J. Zeng, L. Zhang, Y. Yang, G. Zhou, M. Wu, W. Jin, J. Li, and H. Fang, Nature **550**, 380 (2017).
[6]C. Chi, X. Wang, Y. Peng, Y. Qian, Z. Hu, J. Dong, and D. Zhao, Chem. Mater. **28**(9), 2921–2927 (2016).
[7]A. Akbari, P. Sheath, S. T. Martin, D. B. Shinde, M. Shaibani, P. C. Banerjee, R. Tkacz, D. Bhattacharyya, and M. Majumder, Nat. Commun. **7**, 10891 (2016).
[8]M. Ghosh, L. Pradipkanti, V. Rai, D. K. Satapathy, P. Vayalamkuzhi, and M. Jaiswal, Appl. Phys. Lett. **106**(24), 241902 (2015).
[9]M. K. Kavitha, T. Sakorikar, P. Vayalamkuzhi, and M. Jaiswal, Nanotechnology **29**(32), 325706 (2018).
[10]B. Mi, Science **343**(6172), 740–742 (2014).
[11]S. Zheng, Q. Tu, J. J. Urban, S. Li, and B. Mi, ACS Nano **11**(6), 6440–6450 (2017).
[12]C. D. Williams, P. Carbone, and F. R. Siperstein, Nanoscale **10**(4), 1946–1956 (2018).
[13]A. V. Talyzin, T. Hausmaninger, S. You, and T. Szabó, Nanoscale **6**(1), 272–281 (2014).
[14]A. Klechikov, J. Yu, D. Thomas, T. Sharifi, and A. V. Talyzin, Nanoscale **7**(37), 15374–15384 (2015).
[15]C. A. Amadei, A. Montessori, J. P. Kadow, S. Succi, and C. D. Vecitis, Environ. Sci. Technol. **51**(8), 4280–4288 (2017).
[16]K. Nandy, M. J. Palmeri, C. M. Burke, Z. An, S. T. Nguyen, K. W. Putz, and L. C. Brinson, Adv. Mater. Interfaces **3**(6), 1500666 (2016).
[17]J. Y. Chong, B. Wang, C. Mattevi, and K. Li, J. Membr. Sci. **549**, 385–392 (2018).
[18]V. Saraswat, R. M. Jacobberger, J. S. Ostrander, C. L. Hummell, A. J. Way, J. Wang, M. T. Zanni, and M. S. Arnold, ACS Nano **12**(8), 7855–7865 (2018).
[19]Q. Pan, C.-C. Chung, N. He, J. L. Jones, and W. Gao, J. Phys. Chem. C **120**(27), 14984–14990 (2016).
[20]V. Rai, M. K. Kavitha, and M. Jaiswal, presented at the IEEE iNIS-2015, Indore, India (2015).
[21]A. Lipatov, M. J. F. Guinel, D. S. Muratov, V. O. Vanyushin, P. M. Wilson, A. Kolmakov, and A. Sinitskii, Appl. Phys. Lett. **112**(5), 053103 (2018).
[22]I. Jung, D. A. Dikin, R. D. Piner, and R. S. Ruoff, Nano Lett. **8**(12), 4283–4287 (2008).
[23]J. Als-Nielsen and D. McMorrow, *Elements of Modern X-ray Physics* (John Wiley & Sons, Ltd, Singapore, 2011).
[24]A. Ganguly, S. Sharma, P. Papakonstantinou, and J. Hamilton, J. Phys. Chem. C **115**(34), 17009–17019 (2011).
[25]O. Akhavan, Carbon **48**(2), 509–519 (2010).
[26]F. C. Salomão, E. M. Lanzoni, C. A. Costa, C. Deneke, and E. B. Barros, Langmuir **31**(41), 11339–11343 (2015).
[27]M. Jaafar, G. López-Polín, C. Gómez-Navarro, and J. Gómez-Herrero, Appl. Phys. Lett. **101**(26), 263109 (2012).
[28]A. Litke, Y. Su, I. Tranca, T. Weber, E. J. M. Hensen, and J. P. Hofmann, J. Phys. Chem. C **121**(13), 7514–7524 (2017).
[29]N. Raghav, S. Chakraborty, and P. K. Maiti, Phys. Chem. Chem. Phys. **17**(32), 20557–20562 (2015).